Progress on Coronal, Interplanetary, Foreshock, and Outer Heliospheric Radio Emissions

Iver H. Cairns[1], P. A. Robinson[1] and G. P. Zank[2]

[1]School of Physics, University of Sydney, Sydney, NSW 2006, Australia
cairns@physics.usyd.edu.au, robinson@physics.usyd.edu.au
[2]Bartol Research Institute, University of Delaware, Newark, DE 19176, USA
zank@udel.edu

Abstract: Type II and III solar radio bursts are associated with shock waves and streams of energetic electrons, respectively, which drive plasma waves and radio emission at multiples of the electron plasma frequency as they move out from the corona into the interplanetary medium. Analogous plasma waves and radiation are observed from the foreshock region upstream of Earth's bow shock. In situ spacecraft observations in the solar wind have enabled major progress to be made in developing quantitative theories for these phenomena that are consistent with available data. Similar processes are believed responsible for radio emissions at 2–3 kHz that originate in the distant heliosphere, from where the solar wind interacts with the local interstellar medium. The primary goal of this paper is to review the observations and theories for these four classes of emissions, focusing on recent progress in developing detailed theories for the plasma waves and radiation in the source regions. The secondary goal is to introduce and review stochastic growth theory, a recent theory which appears quantitatively able to explain the wave observations in type III bursts and Earth's foreshock and is a natural theory to apply to type II bursts, the outer heliospheric emissions, and perhaps astrophysical emissions.

Keywords: radiation mechanisms: non-thermal—waves—instabilities—Sun: radio radiation—interplanetary medium—shock waves

1 Introduction and Overview

Intense radio emissions are generated in numerous regions of our solar system, including the solar corona and solar wind, regions near shock waves, the magnetospheres and auroral regions of Earth, Jupiter, and the gaseous outer planets, and the regions of the outer heliosphere where the solar wind interacts with the local interstellar medium (see e.g. Melrose 1980, 1986; McLean & Labrum 1985; Benz 1993; Kurth et al. 1984; Gurnett et al. 1993; Zarka 1998). Two basic generation mechanisms are currently believed to be responsible for these emissions, both of them involving collective plasma effects and not the single-particle process of synchrotron emission currently favoured in most theories for astrophysical radio sources. The first mechanism, cyclotron maser emission (Wu & Lee 1979; Melrose 1986; Benz 1993; Zarka 1998), involves the direct generation of x- and o-mode radiation near the electron gyrofrequency f_{ce} or its harmonics by a plasma instability driven by semi-relativistic electrons. This mechanism is believed responsible for radio emissions from the auroral regions of Earth (AKR), Jupiter and the gaseous outer planets

(e.g. Melrose 1976, 1986; Wu & Lee 1979; Zarka 1998), as well as for solar 'spike' bursts in the microwave and decimetric bands (e.g. Melrose 1986; Benz 1993). In each of these source regions, and in general for the mechanism to be effective for direct emission into escaping radiation, the electron gyrofrequency exceeds the electron plasma frequency f_p (i.e. $f_{ce} \geq f_p$) and the electrons have excess energy in their motions perpendicular to the magnetic field. The second mechanism is often called called 'plasma emission' or 'radiation at multiples of the plasma frequency' (Ginzburg & Zheleznyakov 1959; Melrose 1980, 1986; Benz 1993) since it involves the generation of free-space radiation near f_p and near $2f_p$; this mechanism involves a sequence of steps in which excess electron energy is first converted by a plasma instability into electrostatic Langmuir waves with frequencies near f_p, after which Langmuir wave energy is converted into f_p and $2f_p$ radiation by various linear or nonlinear plasma processes.

The primary aim of this paper is to summarise the progress made in the last five years in understanding the generation and properties of type II and III solar radio bursts in the corona and solar wind, radiation from the foreshock region upstream of
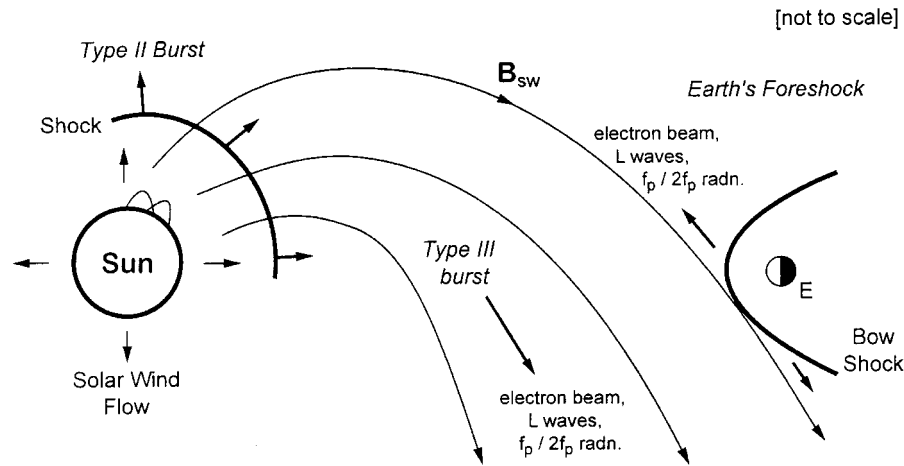
Figure 1—Schematic illustration of the source regions and phenomena involved in type II and III solar radio bursts in the corona and solar wind and those observed in Earth's foreshock.
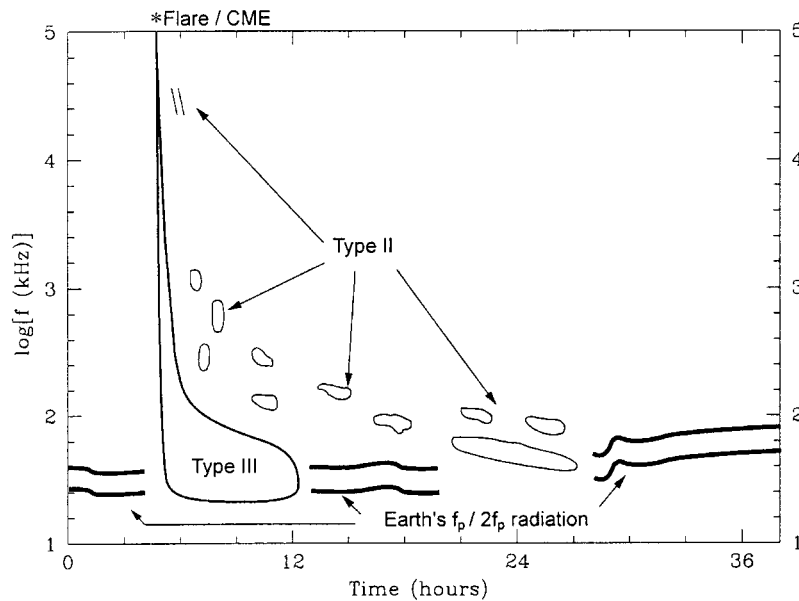

Figure 2—Schematic dynamic spectra for type II and III bursts and the f_p and $2f_p$ radiation from Earth's foreshock.

Earth's bow shock, and low-frequency radiation observed by the Voyager spacecraft in the outer heliosphere. These emissions are all either observed or believed to be radiation produced at multiples of f_p. The properties and source environments of these emissions are briefly introduced next; they are described in more detail in Sections 3–6 below.

For close to 50 years type III bursts have been associated (Figure 1) with electron beams released during solar flares that stream from the corona into the solar wind and drive Langmuir waves and radiation at f_p and $2f_p$ (Wild 1950; Ginzburg & Zheleznyakov 1959), as reviewed by Melrose (1980), Goldman (1983) and Suzuki & Dulk (1985). The electron beams, Langmuir waves and radio emissions have now all been observed in situ (e.g. Gurnett & Anderson 1976; Lin et al. 1981, 1986). Similarly, for over 20 years, the foreshock region upstream

of Earth's bow shock but downstream from the tangent solar wind field line has been observed to contain energetic electrons which stream away from the bow shock, driving Langmuir waves and f_p and $2f_p$ radio emissions. Type II radio bursts have long been interpreted in terms of electron beams accelerated by shock waves (Wild 1950), which then drive Langmuir waves and f_p and $2f_p$ radiation, but observational evidence has been elusive (Nelson & Melrose 1985). Very recently, however, Bale et al. (1999) and Reiner et al. (1997, 1998) have reported convincing evidence that the radiation is produced in an upstream foreshock region, strongly analogous to Earth's foreshock, as suggested previously on theoretical grounds (Cairns 1986a). Figure 2 shows schematic dynamic spectra for these three classes of emissions. Since the type III electrons move at speeds $\sim(0 \cdot 1 – 0 \cdot 3)c$ that are much faster than

the Type II shock ($\sim$500–1000 km s^{-1}), and since the solar wind plasma frequency varies inversely with heliocentric distance R (in steady-state), the type III radiation drifts much more rapidly to low frequencies than the type II radiation. Note that the type III radiation tends to be relatively continuous and broadband, type II bursts tend to be very intermittent but to show distinct f_p and $2f_p$ bands, while the foreshock $2f_p$ radiation is present relatively continuously.
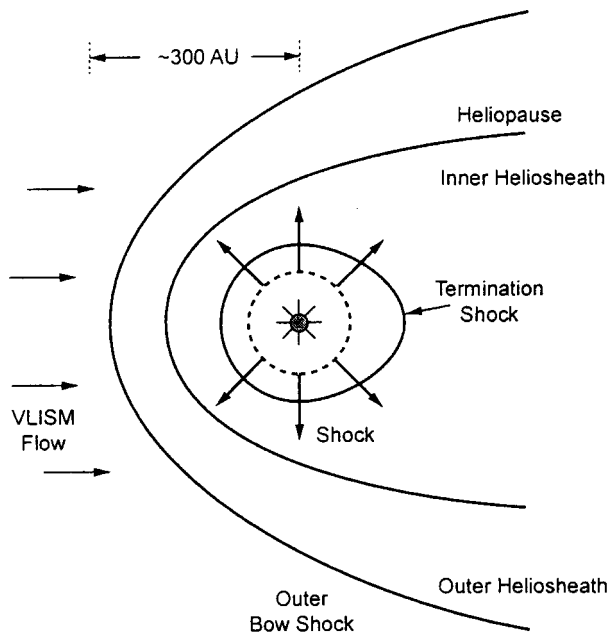

Figure 3—The plasma boundaries associated with the solar wind's interaction with the VLISM: the termination shock, the heliopause, the (possible) outer bow shock, and the inner and outer heliosheath regions inside and outside, respectively, the heliopause. The dashed circle represents a global, transient shock wave, moving away from the Sun into the outer heliosphere, which may drive the outer heliospheric radio emissions.

Figure 3 is a schematic of the large-scale structures predicted to result in the outer heliosphere from the interaction of the super-Alfvenic, supersonic solar wind and the plasma of the very local interstellar medium (VLISM): the solar wind undergoes a shock transition to a sub-Alfvenic flow at the termination shock and is then deflected around the heliopause, a contact discontinuity which separates the (shocked) solar wind and (possibly shocked) VLISM plasmas (e.g. Zank 1999a). An outer bow shock will exist if the VLISM plasma flows super-Alfvenically relative to our solar system. The inner heliosheath, between the termination shock and the heliopause, contains shocked solar wind plasma while the outer heliosheath, between the heliopause and the (possible) outer bow shock, will contain shocked VLISM plasma. The solar system moves relative to the VLISM plasma at a speed

of $\sim$ 26 km s^{-1} along the axis of symmetry in Figure 3, leading to the minimum distances between the Sun and the termination shock, heliopause, etc. lying along this axis. The outer heliospheric radio emissions occur in sporadic, transient outbursts (Kurth et al. 1984, 1987; Gurnett et al. 1993) which have been associated with global shock waves reaching the vicinity of the heliopause and then producing radio emissions (Gurnett et al. 1993); Figure 3 illustrates schematically such a moving shock. Figure 4 shows schematic dynamic spectra for the radio emissions, which are widely interpreted in terms of two components (Cairns, Kurth & Gurnett 1992): the 'transient component' which drifts upwards in frequency with time and the '2 kHz component' which remains approximately fixed in frequency and lasts longer. Current estimates for f_p in the VLISM lie in the range 1·6–3·5 kHz (Zank 1999a).
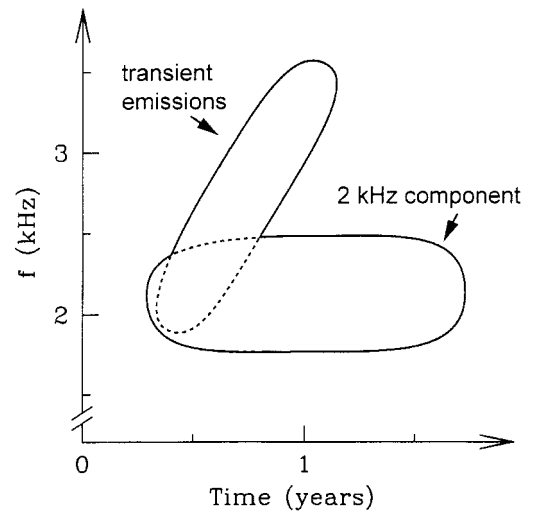

Figure 4—Schematic dynamic spectra of the radio emissions observed by the Voyager spacecraft in the outer heliosphere, showing the transient emissions and the 2 kHz component.

These four classes of emission are naturally grouped together for several reasons, despite their widely different locations and plasma environments. First, type II and III bursts and the foreshock radiation are all observed to be generated near f_p and $2f_p$ in the source region, as is also believed (but not yet demonstrated) for the outer heliospheric emissions. Second, recent observations (Reiner et al. 1998, 1999; Bale et al. 1999) show that interplanetary type II bursts are produced in foreshock regions upstream of certain travelling interplanetary shocks, directly analogous to the radiation from Earth's foreshock, as also postulated for the outer heliospheric emissions (Gurnett et al. 1993; Zank et al. 1994). Third, all four emissions are either observed or believed to be associated with electron beams and the Langmuir waves they drive. Finally, a new theory, stochastic growth theory (SGT), can explain in detail the Langmuir waves and electron beams of type

III bursts and Earth's foreshock (Robinson 1992, 1995; Robinson, Cairns & Gurnett 1993; Cairns & Robinson 1997, 1998, 1999) and is a natural theory to apply to type II bursts and the outer heliospheric radio emissions for the reasons given above. The secondary aim of this paper is to summarise the major ideas of SGT and its successes, an important goal since it is envisaged that SGT may be widely applicable to plasma wave and radiation phenomena in astrophysics and space physics.

The remainder of the paper is structured as follows. Section 2 describes the ideas and theoretical predictions of SGT. Sections 3 to 6 summarise the progress made in understanding the four classes of emissions identified above, as well as the questions that currently remain unanswered. The conclusions are contained in Section 7.

2 Stochastic Growth Theory

Stochastic growth theory describes situations in which an unstable distribution of particles interacts self-consistently with its driven waves in an inhomogeneous plasma environment and evolves to a state in which (1) the particle distribution fluctuates stochastically about a state close to time- and volume-averaged marginal stability, and (2) the fluctuations in the distribution drive waves so that the wave gain $G = 2\ln(E/E_0)$ is a stochastic variable (Robinson 1992, 1995; Robinson, Cairns & Gurnett 1993; Cairns & Robinson 1997, 1999). (Put another way, the wave gain is the time integral of the wave growth rate, being related to the time-varying wave electric field $E(t)$ by $E^2(t) = E_0^2 \exp[G(t)]$ where E_0 is a constant field.) At a given location the postulated stochastic nature of the wave gain means that the wave fields undergo a random walk in $\log E$, whence SGT predicts that the waves occur in bursts with irregular, widely variable fields. Moreover, the closeness to marginal stability means that SGT predicts that the unstable particle distribution and driven waves will persist far from the region where the unstable distribution was first created. SGT is therefore a natural theory to explain the bursty and irregular plasma waves and associated persistence of (marginally) unstable particle distributions that are characteristic of observations in space.

One focus of our current research program is to determine how widely applicable SGT is, with a view to ascertaining whether the combination of SGT and nonlinear wave processes is a broadly applicable paradigm for wave growth in space plasmas. Note that current interpretations of some astrophysical emissions (e.g. radio emissions from pulsars and AGNs) implicitly require preservation of the driving electron distributions for distances much greater than predicted by standard theory to relax the distribution function, thereby perhaps pointing to a role for SGT there.

As required for a theory involving a stochastic variable, the primary observational tests of SGT involve the statistics of the observed wave fields. In particular, for simple SGT systems (in which thermal and nonlinear effects can be neglected and many fluctuations in the distribution occur during a characteristic time for wave growth), SGT predicts via the Central Limit Theorem that the probability distributions of G and $\log E$ should be Gaussian in G and $\log E$ respectively (Robinson 1992, 1995; Robinson, Cairns & Gurnett 1993; Cairns & Robinson 1997, 1999); that is,

$$P(\log E) = \frac{1}{\sqrt{2\pi}\sigma} \exp\left[-\frac{(\log E - \mu)^2}{2\sigma^2} \right]. \quad (1)$$

Here $\mu = \langle \log E \rangle$ is the average of $\log E$ while σ is the standard deviation of $\log E$. Theoretical predictions for the distribution $P(\log E)$ are also known for situations when thermal effects, net linear growth, and nonlinear processes are important (Robinson, Cairns & Gurnett 1993; Robinson 1995) and have been tested successfully (Robinson, Cairns & Gurnett 1993; Cairns, Robinson & Anderson 2000).

It is appropriate to contrast the predictions of SGT with the standard model for wave growth in plasmas (e.g. Stix 1962; Krall & Trivelpiece 1973; Melrose 1986): in the standard model the plasma and unstable particle distribution are homogeneous and the waves undergo exponential growth with a constant growth rate given by homogeneous 'linear' instability theory until the waves reach a level (the threshold) at which one or more nonlinear processes can proceed to saturate the instability and limit the wave fields. The standard model therefore predicts that the $P(\log E)$ distribution should be uniform (or flat) from thermal fields up to the threshold field for the nonlinear processes. [The predictions for $P(\log E)$ above the nonlinear threshold depend on the nature of the nonlinear processes (e.g. Cairns & Robinson 1997, 1999), being either flat, peaked above the nonlinear threshold, or a decreasing power-law tail.] The thresholds for known nonlinear processes can be calculated from analytic plasma theory. It is therefore easy to compare the SGT predictions for the $P(\log E)$ distribution with those of the standard model so as to determine which model, if either, is consistent with observations. A final comment is that the burstiness of the observed waves has no obvious explanation in the standard model, requiring the development of detailed models on a case by case basis, while SGT explains this basic characteristic directly. Conversely, SGT requires an explanation for why the growth is stochastic, typically involving the growth of waves and associated modifications of the unstable particle distribution in an inhomogeneous plasma. Semi-quantitative models for this exist for the Langmuir waves in type III bursts and Earth's foreshock.
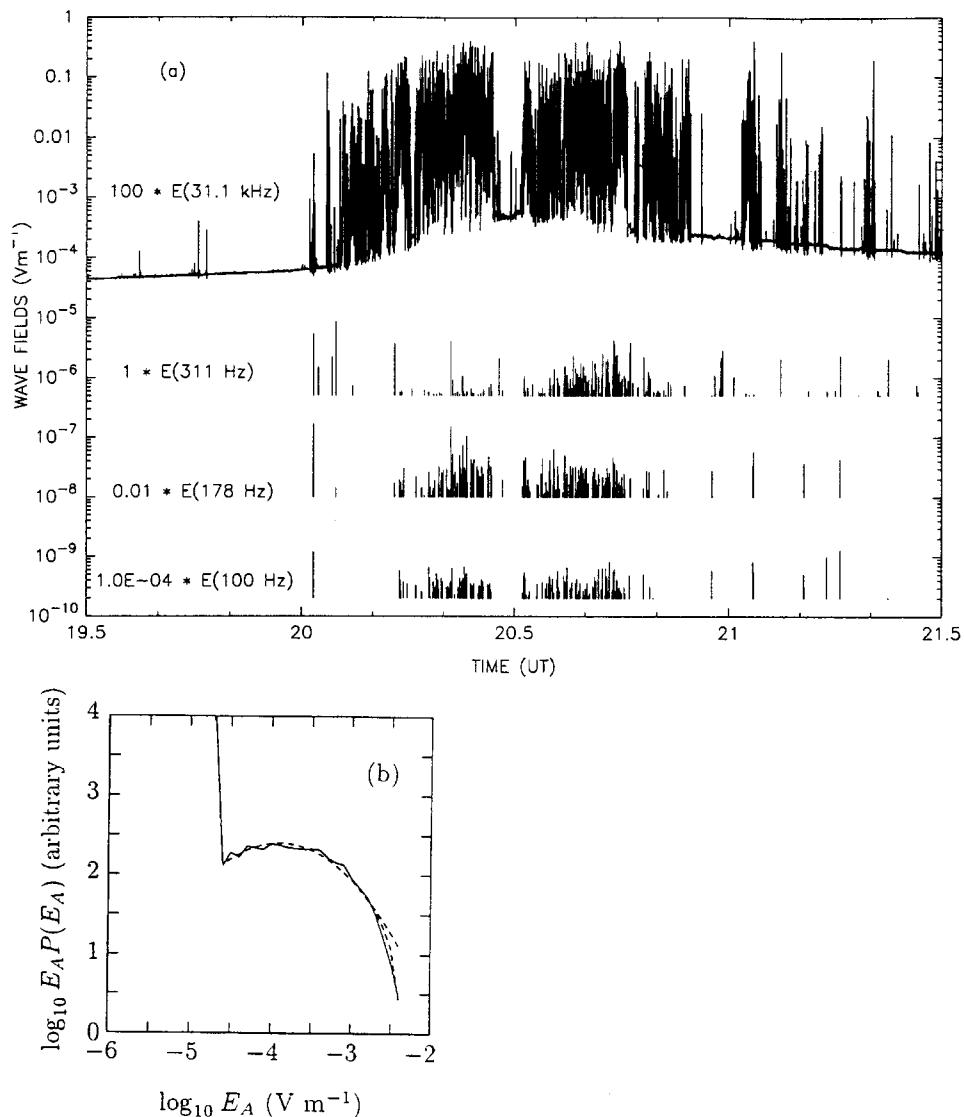
Figure 5—(a) Time-varying electric fields observed by the ISEE-3 spacecraft for bursty Langmuir waves ($31 \cdot 1$ kHz data) and associated ion acoustic-like waves at low frequencies (100—311 Hz data) during a type III burst on 17 February 1979 (Cairns & Robinson 1995a). Electromagnetic radiation from the type III burst provides the smooth, time-varying 'background' in the $31 \cdot 1$ kHz data. (b) Observed probability distribution $P(\log E)$ of wave fields E for the Langmuir data in part (a) is shown as the solid line, while the upper and lower dashed curves show fits to the predictions of SGT without (equation 1) and with, respectively, a nonlinear process active at high fields.

3 Type III Solar Radio Bursts

Type III bursts typically start in the corona at frequencies of order 100 MHz, often as fundamental and harmonic bands differing in frequency by a factor ~ 2, and then drift downwards in frequency as the driving electrons move out into the increasingly dilute plasma of the solar wind (Figures 1 and 2). Interplanetary type III bursts almost never show fundamental/harmonic structure. Both coronal and interplanetary bursts usually have brightness temperatures in excess of 10^{10} K, with a maximum of order 10^{15} K, thereby requiring a coherent emission mechanism. More complete details of the radio emissions and early interpretations are provided in other reviews (Suzuki & Dulk 1985; Melrose 1980; Goldman 1983). It is now well accepted that type III bursts are associated with electron beams (Lin et al. 1981, 1986), which develop as faster electrons outrun slower electrons to form a localised hump in the electron distribution at velocities parallel to the magnetic field which are much larger than the electron thermal speed in the solar wind. Also known as bump-on-tail distributions, these beams drive electrostatic Langmuir waves which are observed to be extremely bursty (see Figure 5a) (Gurnett & Anderson 1976; Lin et al. 1981, 1986; Robinson,
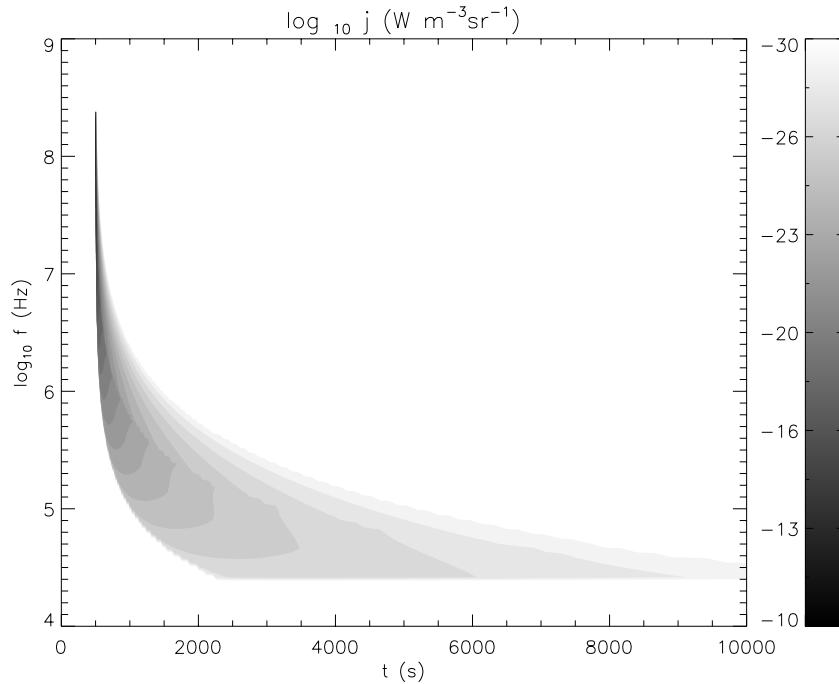
Figure 6—Dynamic spectrum predicted by the detailed SGT model of Robinson & Cairns (1998a,b,c), as described further in the text.

Cairns & Gurnett 1993; Cairns & Robinson 1995a), with electric fields that often vary by more than two orders of magnitude from one sample to the next (separated by $\sim 0 \cdot 5$ s). A fraction of the Langmuir wave energy is transformed into radiation near f_p and $2f_p$.

Figure 5b demonstrates that SGT describes very well the bursty Langmuir waves observed in the source region of one interplanetary type III burst (Robinson, Cairns & Gurnett 1993). The solid curve shows the $P(\log E)$ distribution calculated from the observed wave fields (Figure 5a). The upper dashed curve shows the prediction of equation (1) for simple SGT, while the lower dashed curve shows the SGT prediction including a nonlinear process at high electric fields which removes energy from the Langmuir waves. Excellent agreement between SGT and the data is evident. Figure 5 and similar figures for two other well-observed type III bursts argue strongly that (1) SGT applies and describes the bursty Langmuir waves very well, and (2) a nonlinear process occurs at high fields $E \gtrsim 2$ mV m^{-1}.

In contrast to these successes for SGT, the data are strongly inconsistent with the standard model for plasma wave growth: first, the observed $P(\log E)$ distribution is clearly not flat and, second, most of the wave fields are small compared with the calculated thresholds ≥ 1 mV m^{-1} for nonlinear processes (Robinson, Cairns & Gurnett 1993). Figure 5 is also inconsistent with the strong Langmuir turbulence process of wave collapse saturating the wave growth, since this process should produce a

power-law tail at high E in the $P(\log E)$ distribution (Robinson & Newman 1990). Despite early enthusiasm (Papadopoulos, Goldstein & Smith 1974; Smith, Goldstein & Papadopoulos 1979; Thejappa et al. 1993), detailed tests of collapse theory against the observed Langmuir waves provide multiple strong arguments against collapse occurring frequently or playing a significant role in type III bursts (Robinson, Cairns & Gurnett 1993; Cairns & Robinson 1995b, 1998; Robinson 1997).

In conjunction with SGT, a particular nonlinear process, the Langmuir wave decay $L \rightarrow L' + S$, plays a strong role in explaining the plasma waves and radio emissions of type III bursts; this process involves the decay of a Langmuir wave L into a backward-propagating Langmuir wave L' and an ion acoustic wave S. The threshold field ~ 2 mV m^{-1} inferred from the observed $P(\log E)$ distribution in Figure 5b is consistent with analytic theory for the Langmuir wave decay (Robinson, Cairns & Gurnett 1993). Moreover, the timing and detailed frequencies of a class of low frequency ($\sim$100–500 Hz) waves observed in association with intense bursts of Langmuir waves (Figure 5a) can be explained in terms of S waves produced in the Langmuir wave decay (Robinson, Cairns & Gurnett 1993; Cairns & Robinson 1995a,b). The Langmuir wave decay also produces the backscattered waves L' necessary for the standard $2f_p$ emission process $L + L' \rightarrow T(2f_p)$, where T represents a radio wave, and stimulates the emission of f_p radiation in the process $L \rightarrow T(f_p) + S'$ through the high levels of S waves in the source plasma.

A detailed theory for the dynamic spectra of type III bursts in the corona and solar wind has recently been developed and compared with observations (Robinson & Cairns 1998a,b,c). This theory includes: (1) analytic models for radial and temporal variations in the parameters of the electron beam and the associated energy available for the Langmuir waves; (2) analytic estimates for the efficiencies with which the processes $L \rightarrow L' + S$, $L + L' \rightarrow T(2f_p)$, and $L \rightarrow T(f_p) + S'$ convert Langmuir wave energy into f_p and $2f_p$ radiation, as functions of the beam parameters and wave levels; and (3) analytic descriptions of the large-angle scattering of radiation by density turbulence inside the source and during propagation to the observer. Figure 6 (see Robinson & Cairns 1998b) shows the dynamic spectrum predicted for an observer at 1 AU, with the only inputs being the characteristics of the electron beam and density turbulence obtained from independent data. These predictions closely resemble the observations over the entire frequency range, have volume emissivities and brightness temperatures consistent with observations, can explain the time scales for the exponential rise and decay of radiation at a given frequency from ~ 100 MHz to ~ 30 kHz, and can explain the existence and frequency ratios of fundamental/harmonic bands in the corona and their typical absence in the solar wind.

The SGT theory for type III bursts is thus well developed and has passed successfully all the observational tests yet attempted. So far, however, these detailed tests involve three well-defined type III bursts detected by the ISEE-3 spacecraft, higher time-resolution data from the Ulysses and Galileo spacecraft, and comparisons with the radial and temporal variations and the ranges of observed brightness temperature, volume emissivity, and flux of observed type III bursts (Robinson, Cairns & Gurnett 1993; Cairns & Robinson 1995a,b; Robinson & Cairns 1998a,b,c, and references therein). One question raised recently (see next section) is whether an alternative theory for the radio emission processes, involving linear mode conversion and reflection processes in density gradients, is sometimes relevant. The time is now ripe for testing the SGT theory with (1) a large sample of type III bursts, (2) high time-resolution data on individual Langmuir wave packets from the Wind spacecraft (Bale et al. 1997; Kellogg et al. 1999), and (3) polarisation data.

4 Earth's Foreshock

The Earth's foreshock (see Figure 1) is the region upstream from the bow shock that is downstream of the 3D bundle of magnetic field lines tangent to the shock. The foreshock plasma includes convected solar wind plasma as well as electrons and ions reflected by or leaking through the bow shock.

The reflected particles are energised by shock-drift acceleration at the shock or by Fermi acceleration. In general a convection electric field $\mathbf{E} = -\mathbf{v}_{sw} \times \mathbf{B}_{sw}$ exists in the solar wind, due to the magnetic field $\mathbf{B}_{sw}$ not being aligned with the solar wind velocity $\mathbf{v}_{sw}$. All particles therefore suffer an $\mathbf{E} \times \mathbf{B}$ drift downstream into the foreshock (but perpendicular to the magnetic field), equal in magnitude to the solar wind speed perpendicular to $\mathbf{B}_{sw}$, which restricts particles leaving the shock to lie downstream of the tangent field lines. The gyrocentres of particles in the foreshock move with constant velocity $\mathbf{v}_{\parallel}$ parallel to $\mathbf{B}_{sw}$ and the common $\mathbf{E} \times \mathbf{B}$ drift perpendicular to to $\mathbf{B}_{sw}$. Electron beams are therefore formed naturally in the foreshock due to the spatial variations in $\mathbf{v}_{\parallel}$ required to reach a given location (Filbert & Kellogg 1979; Cairns 1987a), sometimes referred to as 'time-of-flight' effects. Defining D_f as the distance along $\mathbf{v}_{sw}$ from the tangent field line (see Figure 1), with $D_f > 0$ and < 0 in the foreshock and solar wind, respectively, the beam speed (i.e. the minimum parallel speed) required to reach a location increases as $D_f > 0$ decreases. Faster beams are therefore expected closer to the foreshock boundary.

These electron beams are observed to obey the predicted variations in $\mathbf{v}_{\parallel}$ with location D_f (Fitzenreiter, Klimas & Scudder 1984, 1990). These beams drive bursty, irregular Langmuir waves (Filbert & Kellogg 1979; Anderson et al. 1981; Cairns et al. 1997), which persist much further from the bow shock than predicted by standard instability theory and quasilinear theory (Cairns 1987b). Radiation near $2f_p$ is also observed approximately 50% of the time (Hoang et al. 1981). It is difficult to routinely distinguish f_p radiation from thermal noise at f_p, but f_p radiation has been observed (Cairns 1986b; Burgess et al. 1987) and is presumed to be present as often as the $2f_p$ radiation.

Figure 7 (Cairns et al. 1997; Cairns & Robinson 1999) shows how the Langmuir wave fields varied with the coordinate D_f during a period when $\mathbf{B}_{sw}$, the other solar wind parameters, and the locations of the bow shock and global foreshock were either observed or predicted to be unusually slowly varying and constant, thereby allowing temporal and spatial variations in the wave fields to be reliably distinguished. (In general, time variations in $\mathbf{B}_{sw}$ lead to the foreshock sweeping back and forth across a spacecraft, thereby confusing spatial and temporal variations in the wave parameters.) The figure shows weak, thermal Langmuir waves in the solar wind ($D_f < 0$), and then widely varying fields in the foreshock which first increase and then decrease with increasing $D_f > 0$. The estimated error in D_f is only $\pm 0 \cdot 2 \ R_E$. Accordingly, the wide scatter in the wave fields at constant D_f in the foreshock is direct evidence for intrinsic variability

and burstiness of the wave fields at a given location. This provides a prima facie argument that SGT may well be relevant, rather than relying on weaker arguments based upon the analogies between type III bursts and the foreshock waves and the success of SGT at explaining type III bursts.
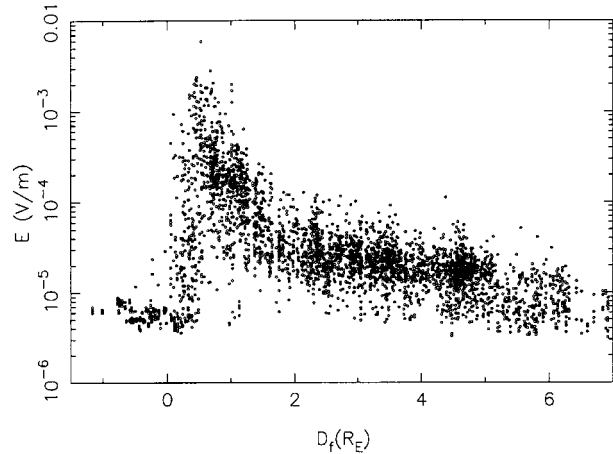

Figure 7—Bursty Langmuir wave fields observed as a function of position in the solar wind ($D_f < 0$) and in Earth's foreshock ($D_f > 0$) during the period 0820–0955 UT on 1 December 1977 (Cairns et al. 1997, 2000; Cairns & Robinson 1997, 1999).

Cairns & Robinson (1999) performed a strong test of SGT over a large fraction of the foreshock using the data of Figure 7. Restricting attention to the region with $D_f > 0 \cdot 6\ R_E$, in which the envelope of wave fields falls off smoothly, they extracted trends in the quantities $\mu(D_f)$ and $\sigma(D_f)$ and then tested SGT using the normalised field variable

$$X = \frac{\log E - \mu(D_f)}{\sigma(D_f)}, \qquad (2)$$

for which equation (1) takes the simple form

$$P(X) = \frac{1}{\sqrt{2\pi}} e^{-X^2/2}. \qquad (3)$$

That is, with these trends extracted, simple SGT predicts that the distribution $P(X)$ should be a Gaussian in X with zero mean, unit standard deviation, and no free parameters. Cairns & Robinson (1999) found that the quantities $E_\mu(D_f) = 10^{\mu(D_f)}$ (the logarithmically-averaged field E) and $\sigma(D_f)$ were both double power-law functions of D_f with a common breakpoint. They then fitted equation (3) to the data of Figure 7 by minimising χ^2 with the double power-law functions for $E_{av}(D_f)$ and $\sigma(D_f)$ as free parameters. Figure 8 shows the SGT prediction equation (3) (solid line) and the distribution $P(X)$ calculated from the data and the fitted power-law functions. The figure provides very strong evidence for SGT. This evidence is strongly

statistically significant according to the standard χ^2 and Kolmogorov–Smirnov tests (Cairns & Robinson 1999). Furthermore, the power-law fits for $E_\mu(D_f)$ and $\sigma(D_f)$ given by the χ^2-minimisation procedure lie within the uncertainty limits given by direct least-squares fits to the data. Thus, simple SGT explains the detailed characteristics of the Langmuir waves in a large fraction of the foreshock.
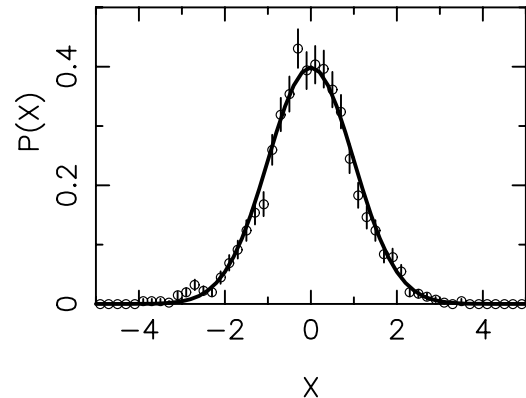

Figure 8—Comparison between observation (symbols with error bars) and the SGT prediction (solid line) for the distribution $P(X)$ of wave fields given by equation (3), as described in detail in the text and by Cairns & Robinson (1999).

Very recently Cairns et al. (2000) applied the predictions of SGT for purely thermal waves and for thermal waves subject to both net linear growth and stochastic growth effects (Robinson 1995) to the Langmuir waves in the solar wind and the edge of the foreshock. This work therefore studied the approach to the pure SGT state demonstrated in Figure 8. Cairns et al. (2000) found that the observed $P(\log E)$ distribution in the solar wind agreed well with the SGT prediction for purely thermal waves, while the $P(\log E)$ distribution observed in the region $0 < D_f < 0 \cdot 6\ R_E$ agreed very well with the SGT prediction for thermal waves subject to net linear growth and stochastic growth effects. Accordingly, the results of Cairns & Robinson (1999) and Cairns et al. (2000) demonstrate that SGT can explain the detailed properties of the Langmuir waves from the solar wind to the deep foreshock, both in the absence of an electron beam and as an electron beam develops and evolves as a function of position in the foreshock.

It is not known what processes produce f_p and $2f_p$ radiation in Earth's foreshock. On the one hand, the Langmuir wave decay and the f_p and $2f_p$ emission processes in the SGT theory for type III bursts have long been hypothesised to produce the foreshock radiation (e.g. Cairns 1988). On the other hand, density turbulence can mode-convert Langmuir waves into f_p radiation and also reflect Langmuir waves so that they can then undergo the standard coalescence $L + L' \to T(2f_p)$ to produce

$2f_p$ radiation (Bale et al. 1998; Yin et al. 1998; Kellogg et al. 1999). SGT can incorporate linear mode conversion and/or the nonlinear processes as the generation mechanisms for the radiation. Further research is required to determine whether the mode conversion/reflection mechanisms provide a viable quantitative alternative to the nonlinear processes in Section 3, both in Earth's foreshock or in type III sources. In the current absence of definitive data, the success of the SGT theory for type III bursts suggests that the Langmuir wave decay and associated f_p and $2f_p$ emission processes should be favoured at the present time.

5 Type II Solar Radio Bursts

Coronal type II solar radio bursts often appear as two bands with a frequency ratio $\sim 1 \cdot 8$–$2 \cdot 0$ in the range ~ 20–400 MHz that drift slowly downwards in frequency at a rate consistent with an MHD shock moving through the solar corona and driving radiation near f_p and $2f_p$ (Wild 1950; Nelson & Melrose 1985). Similar, slow-drift emissions have been observed in the solar wind at frequencies from ~ 20 kHz–20 MHz and directly associated with shock waves measured in situ by spacecraft (Cane et al. 1982, 1987; Lengyel-Frey 1992; Reiner et al. 1997, 1998). It has long been hypothesised that the type II radiation is produced at f_p and $2f_p$ by nonlinear processes involving Langmuir waves which are driven by electron beams accelerated at the shock (Wild 1950; Nelson & Melrose 1985). Indeed, Cairns (1986a) pointed out that in the rest frame of the propagating shock the situation is qualitatively identical to Earth's bow shock and that the reflection/acceleration of electrons into the foreshock region upstream of the type II shock should result naturally in electron beams by the same physics described above for Earth's foreshock. This suggests that a foreshock model for type II bursts is the natural way to develop the theory. However, as described next, multiple unresolved observational questions have hindered the development of a theory for type II bursts and it is only in the last three years that data from the Wind spacecraft have started to clarify the situation significantly.

Direct experimental proof that type II bursts are generated in foreshock sources upstream from shock waves is provided by two recent lines of evidence. First, Reiner et al. (1997, 1998) showed that the frequency of type II radiation varies inversely with time in the solar wind, corresponding to an emitter radiating at f_p and $2f_p$ while moving outward with constant speed in the solar wind (whose density varies inversely with heliocentric distance squared in the steady-state). They found that the radiation frequency reached the local plasma frequency at approximately the same time as an interplanetary, CME-driven shock was observed in situ. These
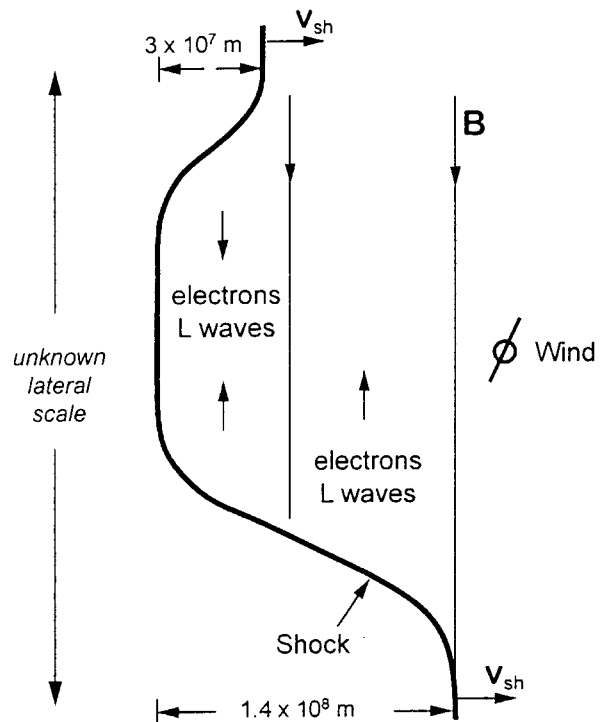

Figure 9—Schematic of the electron streams and Langmuir waves observed, and the detailed foreshock geometry inferred, by Bale et al. (1999) using the first in situ measurements in an active source region of an interplanetary type II burst.

observations are consistent with generation of f_p and $2f_p$ radiation in a foreshock region directly upstream from the shock. However, Reiner et al. (1998) presented no evidence that the spacecraft had passed through an active source region. Second, Bale et al. (1999) provided the first direct observations of energetic electrons and bursty Langmuir waves in an active type II source region upstream of a CME-driven shock. These observations specifically show the production of radiation in a source region moving toward the spacecraft, the arrival of energetic electrons first anti-parallel to **B** and then parallel to **B** which drove high levels of Langmuir waves, and the disappearance of the streaming electrons and Langmuir waves when the shock wave passed over the spacecraft. Figure 9 illustrates these results schematically, demonstrating obvious strong similarities to Earth's foreshock. These direct observations supersede earlier demonstrations that interplanetary type II bursts are statistically strongly associated with fast CME's and interplanetary shock waves (Cane, Shelley & Howard 1987) and that the type II radiation usually has frequencies consistent with generation at f_p and $2f_p$ upstream from a shock (Cane et al. 1982, 1987; Lengyel-Frey 1992).

Unresolved issues include the following:

(1) Do multiple classes of interplanetary type II bursts exist, associated with different spectral properties [broadband, smooth events detected by

ISE-3 (Cane et al. 1982) versus the narrowband, intermittent events measured by Wind (Reiner et al. 1997, 1998)] or shock waves interacting with different structures in the solar wind such as co-rotating interaction regions (CIRs) or dense filaments (Reiner et al. 1997)?

(2) Why are the source regions of interplanetary type II events so rarely encountered and why are most interplanetary and coronal type II events bursty and intermittent?

(3) Why are most coronal and interplanetary type II bursts apparently associated with distinct shocks, as argued on statistical grounds (Gopalswamy et al. 1998), but more compellingly by frequency-time analyses which often show distinct starting times and shock speeds for the coronal and interplanetary exciters (Reiner & Kaiser 1999)? These authors suggest that coronal type II bursts are associated with blast wave shocks while the interplanetary events are generated by CME-driven shocks. A plausible but simple explanation is that perhaps blast waves typically use up their energy (by heating, compressing, and accelerating the plasma particles) and cease to exist at relatively low altitudes, while CMEs provide a large inertia and energy reservoir to drive shocks far into the interplanetary medium.

(4) How are the multiple fine structures (Nelson & Melrose 1985) of coronal and interplanetary type II bursts produced?

(5) Can the combination of SGT and nonlinear processes explain the growth of Langmuir waves and radio emission in type II sources, as expected by analogy with Earth's foreshock and type III bursts?

Further research is required to resolve these issues. It is anticipated that the next few years will lead to a greatly improved theoretical understanding of type II bursts, both in the corona and the solar wind.

6 Outer Heliospheric Radio Emissions

Figure 4 illustrates schematically the radio emissions observed by the Voyager 1 and 2 spacecraft at heliocentric distances greater than 12 AU (Kurth et al. 1984, 1987; Cairns et al. 1992; Gurnett et al. 1993; Gurnett & Kurth 1995). The emissions have occurred in two large outbursts approximately 9–11 years apart, together with some weaker events. The emissions come in two classes, the 'transient' emissions which drift to higher frequencies $\sim 3 \cdot 5$ kHz from initial frequencies $\sim 2 \cdot 4$ kHz over a time period ~ 180 days, and the '2 kHz component' which remains in the frequency range $\sim 1 \cdot 8$–$2 \cdot 4$ kHz and lasts longer than the transient emissions (~ 2 years). These emissions involve emitted powers $\gtrsim 10^{13}$ W and are the most powerful emissions generated in our solar system (Gurnett et al. 1993). In contrast, the radio emissions from the auroral regions and magnetospheres of Jupiter and Earth involve emitted

powers $\lesssim 10^{11}$ W and $\lesssim 10^9$ W, respectively, and the most intense type II and III solar radio bursts involve powers $\lesssim 10^{11}$ W (D. A. Gurnett and M. L. Kaiser, personal communications 1997). Noting that the power in the solar wind's kinetic energy flux is $\sim 5 \times 10^{16}$ W, it appears that a global interaction involving the solar wind is a natural way to account for the observed power.

McNutt (1988) suggested that the emissions are triggered by the arrival of solar wind disturbances in the vicinity of the termination shock or the heliopause. First interpreted in terms of unusually fast solar wind streams, the trigger is now widely accepted to be a fast-moving global region of compressed magnetic field and density which drives a shock in the outer heliosphere (Gurnett et al. 1993). These so-called global merged interaction regions (Burlaga et al. 1991), or GMIRs, result from the merging of multiple CMEs and associated shocks and magnetic field enhancement, produced by solar activity, in the distant solar wind beyond about 20 AU. The GMIRs produce major decreases in the flux of cosmic rays and other energetic particles (Forbush decreases), due to scattering and mirroring effects by the GMIR's enhanced and turbulent magnetic fields, that are observed as the GMIR passes the Earth and spacecraft. Gurnett et al. (1993) and Gurnett & Kurth (1995) demonstrated that the two major outbursts of radio emission started approximately 415 days after the two largest Forbush decreases measured thus far at Earth and that a GMIR with associated Forbush decreases and a shock wave was observed by multiple widely-spaced spacecraft between 1 and 53 AU for each radio event. Moreover, taking into account the measured shock speeds ~ 800–850 km s^{-1}, the observed time delays ~ 415 days, and plausible estimates for slowing of the shock beyond the termination shock, Gurnett et al. (1993) estimated that the source region lies ~ 110—180 AU from the Sun. These distances are plausible for the heliopause (see e.g. Zank 1999a).

The Gurnett et al. (1993) model for the radio emissions thus involves the GMIR shock starting to produce f_p and $2f_p$ emission after it traverses the heliopause: the transient emissions come from a putative density enhancement near the nose of the heliopause, while the 2 kHz component comes from other regions of the outer heliosheath. Figures 3 and 10 illustrate this model, which can be tested directly using the output from global plasma simulations of the outer heliosphere (Zank 1999a, and references therein) and a model for a shock's propagation through the outer heliosphere. The variations in f_p with heliocentric distance predicted by the Zank et al. (1996) global simulation code are shown in Figure 10; this simulation uses input parameters for the plasma and neutral characteristics of the solar wind and VLISM obtained from published

observations. Current estimates for f_p in the VLISM are $1 \cdot 6$–$3 \cdot 5$ kHz (Zank 1999a). Figure 11 shows the dynamic spectrum predicted for a GMIR shock that produces f_p and $2f_p$ radiation in an upstream foreshock as it moves through the global 3D plasma structures obtained from the Zank et al. (1996) simulation code (Cairns & Zank 1999). The shock is assumed to leave the Sun at the time origin and to move at a constant, isotropic speed of 600 km s^{-1}.
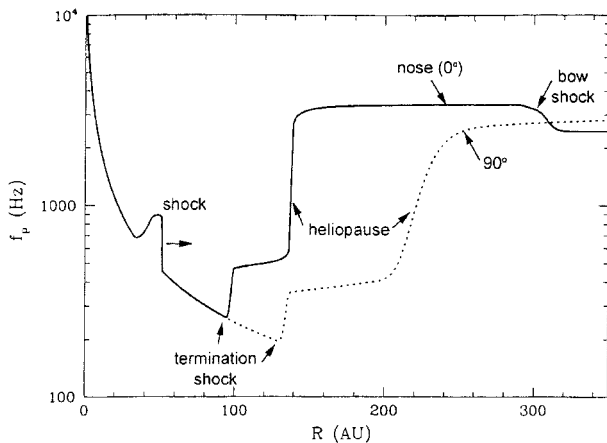

Figure 10—Profiles of f_p as a function of heliocentric distance R predicted by global simulations (Zank et al. 1996) along the nose direction, defined by the VLISM's velocity vector relative to our solar system, and at right-angles to that direction. These profiles have been modified near $R \sim 50$ AU by superposing the GMIR-driven shock wave hypothesised to produce the outer heliospheric radiation as f_p and/or $2f_p$ radiation near and beyond the heliopause.

A number of emissions can be identified in Figure 11 (Cairns & Zank 1999). First, the emissions below 500 Hz prior to day 280 are f_p and $2f_p$ emission from the undisturbed solar wind (the shock reaches the nose of the termination shock on day 280) while the emissions below 1 kHz after day 280 are $2f_p$ emissions from the inner heliosheath (the band from 500 Hz to 1 kHz) and the superposition of f_p emission from the inner heliosheath with emission from regions of the shock still in the undisturbed solar wind. Second, the relatively weak emissions drifting rapidly to higher frequencies (ranging from ~ 1 to 6 kHz) are produced when the shock moves up the density ramp at the heliopause (see Figure 10b). Different stripes correspond to emission from different angles θ relative to the axis direction in Figure 3. Third, the intense, relatively broadband, and slowly varying emissions in two bands with frequencies ~ 3 and 6 kHz are produced when the shock is in the outer heliosheath beyond the heliopause.

Comparing Figures 4 and 11, it is very appealing to interpret the 2 kHz component as f_p radiation produced in the outer heliosheath, consistent with the Gurnett et al. (1993) model (Cairns & Zank 1999). Note that current estimates of f_p in the VLISM are

$\sim 1 \cdot 6$–$3 \cdot 5$ kHz (Zank 1999a), not inconsistent with Figure 11 and f_p in the Zank et al. (1996) simulations. In contrast, the only upward-drifting emissions in Figure 11 occur when the shock moves up the density ramp at the heliopause; these emissions drift far too rapidly to be consistent with the observed time scale of transient emissions (~ 180 days). A detailed explanation for the transient emissions therefore does not exist at the present time (Cairns & Zank 1999).

The simplest qualitative interpretation remains that transient emissions are generated when a GMIR shock moves up a density ramp beyond the heliopause (e.g. Gurnett et al. 1993), but the location and nature of the density ramp need to be identified. With the the heliopause density ramp itself apparently ruled out by Figure 11 (Cairns & Zank 1999) and the absence of the Gurnett et al. (1993) putative density ramp in current steady-state simulations (Zank et al. 1996; Linde et al. 1998), new ideas are required. One possibility is that solar cycle effects lead to the generation of large scale density waves in the outer heliosheath (Zank 1999b) and that traversal of the density waves by the GMIR shock leads to the observed transient emissions. Further work on the theory and simulation of these emissions and the outer heliosphere is required, including the possible role of SGT, as well as on in situ observations of the plasmas, global plasma structures, and radio source regions in the outer heliosphere by the Voyager spacecraft and their successors.

7 Conclusions

SGT provides a natural, quantitatively testable theory for bursty plasma waves and radio emissions associated with unstable particle distributions that persist far from their source. The combination of SGT and specific nonlinear processes provides a detailed, quantitative theoretical explanation for the persistent electron beams, bursty Langmuir waves, and radiation of solar type III bursts in the corona and solar wind. SGT also accounts quantitatively for the bursty Langmuir waves and electron beams in Earth's foreshock. Further work is required to determine, whether the nonlinear processes in the current theory for type III bursts produce the foreshock radiation, or whether the combination of linear mode conversion and reflection in density turbulence with the standard $2f_p$ coalescence is a viable alternative. This second option should also be considered for type III bursts. Very recent work demonstrates that many, perhaps all, interplanetary type II bursts are generated in foreshock regions upstream of shock waves driven by CMEs, as has long been suspected. These observations show streaming electrons, bursty Langmuir waves and f_p and $2f_p$ radiation that are qualitatively analogous to those in Earth's foreshock. This suggests that SGT will
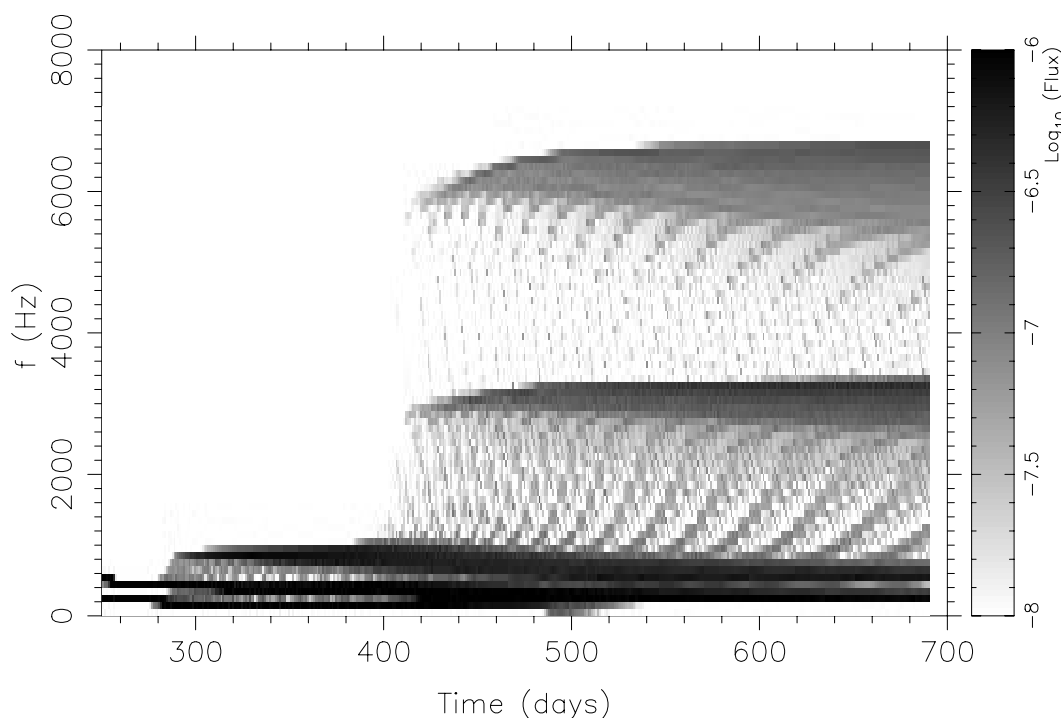
Figure 11—Theoretical predictions (Cairns & Zank 1999) for the dynamic spectra of radio emissions generated at f_p and $2f_p$ upstream of a shock moving isotropically at 600 km s^{-1} through the plasma environment given by the global simulations of Zank et al. (1996).

eventually provide a detailed explanation for type II bursts. The two classes of radio emissions generated in the outer heliosphere (transient emissions and the 2 kHz component) are also interpreted in terms of f_p and $2f_p$ radiation generated in foreshock regions, in this case upstream of shocks driven by global merged interaction regions near the heliopause. Detailed calculations using global simulations to predict the 3D plasma density in the outer heliosphere suggest that this model can explain the 2 kHz component as f_p emission from beyond the heliopause. However, the calculations cannot explain the observed durations of the transient emissions. The research reported here on four classes of radio emissions in our solar system suggests that SGT may indeed be widely applicable to plasma waves and radio emissions in our solar system and thereby, potentially at least, to astrophysical sources.

Acknowledgments

References

Anderson, R. R., Parks, G. K., Eastman, T. E., et al. 1981, J. Geophys. Res., 86, 4493

Bale, S. D., Burgess, D., Kellogg, P. J., et al. 1997, J. Geophys. Res., 102, 11,281

Bale, S. D., Kellogg, P. J., Goetz, K., et al. 1998, Geophys. Res. Lett., 25, 9

Bale, S. D., Reiner, M. J., Bougeret, J.-L., et al. 1999, Geophys. Res. Lett., 26, 1573

Benz, A. O. 1993, Plasma Astrophysics (Amsterdam: Kluwer)

Burgess, D., Harvey, C. C., Steinberg, J. L., et al. 1987, Nature, 330, 732

Burlaga, L. F., McDonald, F. B., Ness, N. F., et al. 1991, J. Geophys. Res., 96, 3780

Cairns, I. H. 1986a, PASA, 6, 444

Cairns, I. H. 1986b, J. Geophys. Res., 91, 2975

Cairns, I. H. 1987a, J. Geophys. Res., 92, 2315

Cairns, I. H. 1987b, J. Geophys. Res., 92, 2329

Cairns, I. H. 1988, J. Geophys. Res., 93, 3958

Cairns, I. H., & Robinson, P. A. 1995a, ApJ, 453, 959

Cairns, I. H., & Robinson, P. A. 1995b, Geophys. Res. Lett., 22, 3437

Cairns, I. H., & Robinson, P. A. 1997, Geophys. Res. Lett., 24, 369

Cairns, I. H., & Robinson, P. A. 1998, ApJ, 509, 471

Cairns, I. H., & Robinson, P. A. 1999, Phys. Rev. Lett., 82, 3069

Cairns, I. H., & Zank, G. P. 1999, Geophys. Res. Lett., 26, 2605

Cairns, I. H., Kurth, W. S., & Gurnett, D. A. 1992, J. Geophys. Res., 97, 6245

Cairns, I. H., Robinson, P. A., & Anderson, R. R. 2000, Geophys. Res. Lett., 27, 61

Cairns, I. H., Robinson, P. A., Anderson, R. R., et al. 1997, J. Geophys. Res., 102, 24,249

Cane, H. V., Sheeley, N. R. Jr., & Howard, R. A. 1987, J. Geophys. Res., 92, 9869

Cane, H. V., Stone, R. G., Fainberg, J., et al. 1982, Sol. Phys., 78, 187

Filbert, P. C., & Kellogg, P. J. 1979, J. Geophys. Res., 84, 1369

Fitzenreiter, R. J., Klimas, A. J., & Scudder, J. D. 1984, Geophys. Res. Lett., 11, 496

Fitzenreiter, R. J., Klimas, A. J., & Scudder, J. D. 1990, J. Geophys. Res., 95, 4155

Ginzburg, V. L., & Zheleznyakov, V. V. 1959, Sov. Astron. J., 3, 255

Goldman, M. V. 1983, Sol. Phys., 89, 403

Gopalswamy, N., Kaiser, M. L., Lepping, R. P., et al. 1998, J. Geophys. Res., 103, 307

Gurnett, D. A., & Anderson, R. R. 1976, Science, 194, 1159

Gurnett, D. A., & Kurth, W. S. 1995, Adv. Space Res., 16(9), 279

Gurnett, D. A., Kurth, W. S., Allendorf, S. C., et al. 1993, Science, 262, 199

Hoang, S., Fainberg, J., Steinberg, J.-L., et al. 1981, J. Geophys. Res., 84, 4531

Kellogg, P. J., Goetz, K., Monson, S. J., et al. 1999, J. Geophys. Res., 104, 17,069

Krall, N. A., & Trivelpiece, A. W. 1973, in Principles of Plasma Physics (New York: McGraw–Hill)

Kurth, W. S., Gurnett, D. A., Scarf, F. L., et al. 1984, Nature, 312, 27

Kurth, W. S., Gurnett, D. A., Scarf, F. L., et al. 1987, Geophys. Res. Lett., 14, 49

Lengyel-Frey, D. 1992, J. Geophys. Res., 97, 1609

Lin, R. P., Potter, D. W., Gurnett, D. A., et al. 1981, ApJ, 251, 364

Lin, R. P., Levedahl, W. K., Lotko, W. K., et al. 1986, ApJ, 308, 954

Linde, T. J., Gombosi, T. I., et al. 1998, J. Geophys. Res., 103, 1889

McLean, D. J., & Labrum, N. R. 1985, Solar Radiophysics (Cambridge Univ. Press)

McNutt, R. L., Jr 1988, Geophys. Res. Lett., 15, 1307

Melrose, D. B. 1976, ApJ, 207, 651

Melrose, D. B. 1980, Plasma Astrophysics, Vols I and II (New York: Gordon & Breach)

Melrose, D. B. 1986, Instabilities in Space and Laboratory Plasmas (Cambridge Univ. Press)

Nelson, G. J., & Melrose, D. B. 1985, in Solar Radiophysics, ed. D. J. McLean & N. R. Labrum (Cambridge Univ. Press)

Papadopoulos, K. D., Goldstein, M. L., & Smith, R. A. 1974, ApJ, 190, 175

Reiner, M. J., & Kaiser, M. L. 1999, J. Geophys. Res., 104, 16,979

Reiner, M. J., Kaiser, M. L., Fainberg , J., et al. 1997, in Correlated Phenomena at the Sun, in the Heliosphere, and in Geospace, Proc. 31st ESLAB Symp., ESTEC, Nordwijk

Reiner, M. J., Kaiser, M. L., Fainberg, J., et al. 1998, J. Geophys. Res., 103, 29,651

Robinson, P. A. 1992, Sol. Phys., 139, 147

Robinson, P. A. 1995, Phys. Plasmas, 2, 1466

Robinson, P. A. 1997, Rev. Mod. Phys., 69, 507

Robinson, P. A., & Cairns, I. H. 1998a, Sol. Phys., 181, 363

Robinson, P. A., & Cairns, I. H. 1998b, Sol. Phys., 181, 395

Robinson, P. A., & Cairns, I. H. 1998c, Sol. Phys., 181, 429

Robinson, P. A., & Newman, D. L. 1990, Phys. Fluids B, 2, 2999

Robinson, P. A., Cairns, I. H., & Gurnett, D. A. 1993, ApJ, 407, 790

Smith, R. A., Goldstein, M. L., & Papadopoulos, K. D. 1979, ApJ, 234, 348

Stix, T. H. 1962, The Theory of Plasma Waves (New York: McGraw–Hill)

Suzuki, S., & Dulk, G. A. 1985 in Solar Radiophysics, ed. D. J. McLean & N. R. Labrum (Cambridge Univ. Press)

Thejappa, G., Lengyel-Frey, D., Stone, R. G., et al. 1993, ApJ, 416, 831

Wild, J. P. 1950, Aust. J. Sci. Res., A3, 541

Wu, C. S., & Lee, L. C. 1979, ApJ, 230, 621

Yin, L., Ashour-Abdalla, M., El-Alaoui, M., et al. 1998, Geophys. Res. Lett., 25, 2513

Zank, G. P. 1999a, Space Sci. Rev., 89 (3/4), 1

Zank, G. P. 1999b, in Solar Wind Nine, ed. S. R. Habbal et al., AIP Conf. Proc. 471 (New York: AIP)

Zank, G. P., Cairns, I. H., Donohue, D. J., & Matthaeus, W. H. 1994, J. Geophys. Res., 90, 14,729

Zank, G. P, Pauls, H. L., Williams, L. L., & Hall, D. T. 1996, J. Geophys. Res., 101, 21,639

Zarka, P. 1998, J. Geophys. Res., 103, 20,159